CrystEngComm

RSC Publishing

PAPER

# Synthesis of polycrystalline cobalt selenide nanotubes and their catalytic and capacitive behaviors†

Cite this: *CrystEngComm*, 2013, **15**, 5928

Zhenghua Wang,* Qiang Sha, Fengwei Zhang, Jun Pu and Wu Zhang*

Received 24th January 2013,
Accepted 20th May 2013

DOI: 10.1039/c3ce40152a

**www.rsc.org/crystengcomm**

Polycrystalline $Co_{0.85}Se$ nanotubes are successfully prepared by using $Co(CO_3)_{0.35}Cl_{0.20}(OH)_{1.10}$ nanorods as precursor through a solvothermal process. The as-prepared $Co_{0.85}Se$ nanotubes show efficient catalytic performance for decomposition of hydrazine hydrate at room temperature. The catalysts can be repeatedly used and their repeatability is also excellent. The $Co_{0.85}Se$ nanotubes can also be applied as supercapacitor electrode materials. Galvanostatic charge–discharge measurements show that the $Co_{0.85}Se$ nanotube electrode has a specific capacitance of 238 F $g^{-1}$ at a current density of 1 A $g^{-1}$ after 100 cycles of activation, and retaining 90.3% of the capacitance after the next 1900 cycles.

## 1 Introduction

As an important transition metal chalcogenide, cobalt selenide has attracted much attention due to its important applications in many areas such as solar cells, catalysts, and wastewater treatment.[1–6] Cobalt selenide has a variety of compounds such as $CoSe_2$, CoSe, $Co_{0.85}Se$, $Co_3Se_4$ and $Co_2Se_3$.[7–12] Cobalt selenide nanomaterials have been prepared by diverse methods including hydrothermal method,[9] solvothermal method,[10] microwave-assisted polyol process,[12] mechanical alloying,[13] and potentiostatic electrodeposition route.[14] However, to date, synthesis of cobalt selenide nanotubes and their application as electrochemical supercapacitor electrode materials have rarely been reported.

In recent years, electrochemical supercapacitors have been a new research hot spot in the energy storage area due to their advantages of high power density, high specific energy density, fast charging–discharging rates, long cycle life and so forth, compared to rechargeable batteries and conventional dielectric capacitors. The materials studied for capacitor electrodes are mainly of three types: carbon,[15–18] metal oxide,[19–21] and electronically conducting polymers.[22,23] Carbon materials (activated carbon, carbon nanotube, graphene, *etc.*) are widely used for electric double-layer capacitors. Metal oxides and conducting polymer are widely used for pseudocapacitors. In general, the pseudocapacitors show higher energy density than the electric double-layer capacitors. $RuO_2$ is widely studied as a pseudocapacitor electrode material with very high specific capacitance.[24] However, its high cost and low abundance limits its practical application. Other transition metal oxides such as $MnO_2$,[25] NiO,[26] and $Co_3O_4$ (ref. 27) have also been studied. These electrode materials show limited energy density than $RuO_2$. Conducting polymer-based materials also have some disadvantages such as a lower cycle life and slow ion transport kinetics. Therefore, the development of alternative supercapacitor electrode materials with low cost and improved performance is of great importance.

Hydrazine has been widely used in many fields. The decomposition of hydrazine is particularly important for a number of industrial and scientific research areas including monopropellant satellite thrusters, gas generators, and pure hydrogen production for fuel cells. One of the best commercial catalysts for hydrazine decomposition is the $Ir/Al_2O_3$ (Shell 405) catalyst. However, iridium is very rare and expensive. Hence, researchers have turned to developing cheaper catalysts. Some transition metal compounds such as cobalt selenide ($Co_{0.85}Se$),[3] tungsten carbide (WC),[28] and molybdenum nitride ($Mo_2N$)[29] have been reported for catalytic hydrazine decomposition.

In this paper, we report a simple template-directed route for the preparation of polycrystalline $Co_{0.85}Se$ nanotubes under solvothermal conditions. The $Co_{0.85}Se$ nanotubes can be applied as an efficient catalyst for decomposition of hydrazine hydrate in water at room temperature, and can be repeatedly used with stable catalytic activity. An electrode made from $Co_{0.85}Se$ nanotubes exhibits a specific capacitance of 238 F $g^{-1}$ at a current density of 1 A $g^{-1}$ in 1 M KOH, and a low capacitance loss of 9.7% after 2000 cycles. A comparison between the $Co_{0.85}Se$ nanotubes and nanoparticles reveals that the $Co_{0.85}Se$ nanotubes have better catalytic and capacitive properties. These results show that the $Co_{0.85}Se$ nanotubes are promising for application in the fields of catalysis and supercapacitor.

*Anhui Key Laboratory of Functional Molecular Solids, College of Chemistry and Materials Science, Anhui Normal University, Wuhu 241000, P. R. China. E-mail: zhwang@mail.ahnu.edu.cn; wuzhang@mail.ahnu.edu.cn; Fax: +86-553-3869302; Tel: +86-553-3869303*

† Electronic supplementary information (ESI) available: XRD and FESEM images of $Co_{0.85}Se$ nanoparticles. See DOI: 10.1039/c3ce40152a

## 2 Experimental

All chemical reagents were of analytical grade and were used without further purification.

### 2.1 Synthesis of $Co(CO_3)_{0.35}Cl_{0.20}(OH)_{1.10}$ nanorods

$Co(CO_3)_{0.35}Cl_{0.20}(OH)_{1.10}$ nanorods are used as a precursor for the preparation of $Co_{0.85}Se$ nanotubes. The procedure for the synthesis of $Co(CO_3)_{0.35}Cl_{0.20}(OH)_{1.10}$ nanorods has been reported by us previously,[30] as summarized following: $CoCl_2{\cdot}6H_2O$ (1.190 g, 0.005 mol) and $CO(NH_2)_2$ (0.300 g, 0.005 mol) were dissolved in 50 mL deionized water together, then the solution was transferred into a Teflon lined stainless steel autoclave with a capacity of 60 mL and heated at 120 °C for 10 h. After that, the autoclave was cooled to room temperature naturally. The pink precipitates were filtered off, washed with deionized water and absolute ethanol for several times each, and then dried in vacuum at 60 °C for 2 h.

### 2.2 Preparation of NaHSe solution

Firstly, $NaBH_4$ (0.080 g, 0.002 mol) was dissolved in 2 mL deionized water in a glass bottle. Then, Se powder (0.079 g, 0.002 mol) was added into the glass bottle. The glass bottle was sealed and gently shaken until the black Se powder was completely dissolved and a milky solution was obtained.

### 2.3 Synthesis of $Co_{0.85}Se$ nanotubes

In a typical procedure, 0.107 g of the $Co(CO_3)_{0.35}Cl_{0.20}(OH)_{1.10}$ sample and 2 mL of freshly prepared NaHSe solution were loaded into a Teflon lined stainless steel autoclave of 60 mL capacity, and then the autoclave was filled with ethanol up to 80% of its total volume. The autoclave was heated at 140 °C for 8 h, and then cooled to room temperature naturally. The black precipitates were filtered off, washed with deionized water and absolute ethanol for several times each, and dried in a vacuum at 60 °C for 2 h.

As a comparison, $Co_{0.85}Se$ nanoparticles were prepared by substituting $Co(CO_3)_{0.35}Cl_{0.20}(OH)_{1.10}$ with $CoCl_2{\cdot}6H_2O$ while the other conditions were kept unchanged.

### 2.4 Characterizations

X-ray powder diffraction (XRD) patterns were obtained on a Japan Rigaku D/max-γ B X-ray diffractometer equipped with graphite monochromatized Cu Kα radiation ($\lambda$ = 0.154187 nm). X-ray photoelectron spectra (XPS) were obtained on an ESCALab MKII X-ray photoelectron spectrometer with non-monochromatized Mg Kα X-ray as the excitation source. The binding energies in XPS analysis were corrected by referencing C 1s to 284.60 eV. The field emission scanning electron microscopy (FESEM) images were taken with a Hitachi S-4800 scanning electron microscope. The transmitting electron microscopy (TEM) images and energy dispersive X-ray spectrum (EDX) were recorded on a FEI Tecnai $G^2$ 20 high-resolution transmission electron microscope performed at an acceleration voltage of 200 kV.

### 2.5 Catalytic activity measurements

The catalytic degradation of hydrazine hydrate was conducted according to the following procedure: the as-prepared $Co_{0.85}Se$ sample (0.050 g) was dispersed into an aqueous solution of hydrazine hydrate (0.002 M, 50 mL) at room temperature (about 25 °C), and then the solution was placed in the dark and stirred vigorously with a magnetic stirrer. At intervals of 10 min, 3 mL of the suspension was taken out, centrifuged, and the supernatant liquid was collected for further characterization.

The concentration of hydrazine hydrate was measured spectrophotometrically according to a previous report with minor modifications.[31] The color reagent was composed of *p*-dimethylaminobenzaldehyde (8 g), ethanol (50.0 mL), and concentrated hydrochloric acid (50.0 mL). In a typical procedure, 0.5 mL supernatant liquid, 2.5 mL color reagent and 22.0 mL distilled water were mixed together and left for 10 min. Then the mixed solution was measured with a Shimadzu UV-3010 spectrometer. The concentration of hydrazine hydrate was determined from the calibration curve which was constructed beforehand.

### 2.6 Electrochemical measurements

The capacitive performances of the as-prepared $Co_{0.85}Se$ sample were measured on a CHI 660D electrochemical working station (ChenHua Corp., Shanghai, China) with a three electrode experimental setup. The working electrode was prepared by pasting a slurry mixture of the as-prepared $Co_{0.85}Se$ sample (80 wt%), acetylene black (15 wt%) and polytetrafluoroethylene binder (5 wt%) using ethanol as solvent onto a piece of nickel foam, and dried under vacuum at 50 °C for 6 h. Platinum wire and standard calomel electrode (SCE) were used as the counter and reference electrodes in a 1 M KOH solution, respectively. Cyclic voltammetry (CV) was performed within a potential range from 0 to 0.5 V at scan rates from 10 to 200 mV $s^{-1}$. The galvanostatic charge–discharge characteristics were tested at current densities of 1, 2, 4 and 8 A $g^{-1}$. The electrochemical impedance spectroscopies (EIS) were conducted by applying a sine wave with an amplitude of 5.0 mV in the frequency range of 100 kHz to 0.1 Hz.

### 2.7 Electrochemical calculations

1. Specific capacitances derived from charge–discharge tests can be calculated from the following equation:[32]

$$C = \frac{I \times \Delta t}{m \times \Delta V} \quad (1)$$

where $C$ (F $g^{-1}$) is the specific capacitance of the electrode based on the mass of active materials, $I$ (A) is the current during discharge process, $\Delta t$ (s) is the discharge time, $\Delta V$ (V) is the potential window (here $\Delta V$ = 0.5 V), $m$ (g) is the mass of active materials.

2. Energy density and power density derived from charge–discharge tests can be calculated from the following equations:[33]

$$E = \frac{1}{2} CV^2 \quad (2)$$

$$P = \frac{E}{t} \quad (3)$$

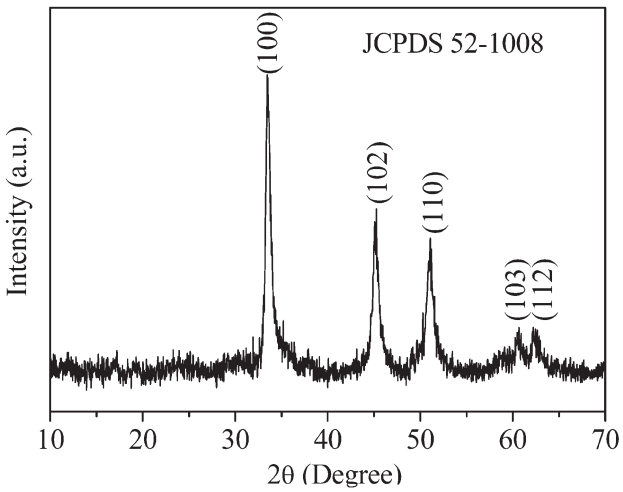


**Fig. 1** XRD pattern of the $Co_{0.85}Se$ sample.

where $E$ (Wh $kg^{-1}$) is the average energy density; $C$ (F $g^{-1}$) is the specific capacitance; $V$ (V) is the potential window (here $\Delta V$ = 1.5 V); $P$ (W $kg^{-1}$) is the average power density and $t$ (s) is the discharge time.

## 3 Results and discussion

The phase, crystallinity and purity of the as-obtained sample were examined by the XRD technique. Fig. 1 shows a typical XRD pattern of the sample obtained from the reaction of the precursor sample with NaHSe solution. All of the reflection peaks in this pattern can be readily indexed to hexagonal $Co_{0.85}Se$ (JCPDS card No. 52-1008). The broad reflection peaks indicate the small size of the samples. No diffraction peaks corresponding to the precursor can be seen in this pattern, which indicates that the precursor has been totally converted into $Co_{0.85}Se$.

The chemical bonding states of each element on the surface of $Co_{0.85}Se$ sample were evaluated by the XPS technique. The XPS survey spectrum indicates the presence of Co and Se as well as C and O absorbed due to exposure to the air. Fig. 2a shows the core level spectrum of the Co 2p region, in which the Co $2p_{3/2}$, $2p_{1/2}$, and two satellite peaks (marked as "Sat.") are seen. These peaks are computer fitted and two spin–orbit doublets characteristic of $Co^{2+}$ and $Co^{3+}$ are considered. The binding energies of $Co^{2+}$ $2p_{3/2}$, $Co^{3+}$ $2p_{3/2}$, $Co^{2+}$ $2p_{1/2}$ and $Co^{3+}$ $2p_{1/2}$ are 780.9, 779.0, 797.2 and 794.0 eV, respectively, which are in good agreement with the reported values.[34] This result shows that the cobalt elements on the surface of the as-synthesized $Co_{0.85}Se$ sample have two types of oxide states, *i.e.* $Co^{2+}$ and $Co^{3+}$. Fig. 2b shows the core level spectrum of the Se 3d region. The binding energy of 55.4 eV is close to the reported value.[35]

The morphology of the as-prepared samples was examined by FESEM. Fig. 3a and b show FESEM images of the precursor with different magnification, from which we learn that the precursor is composed of many nanorod bunches. The

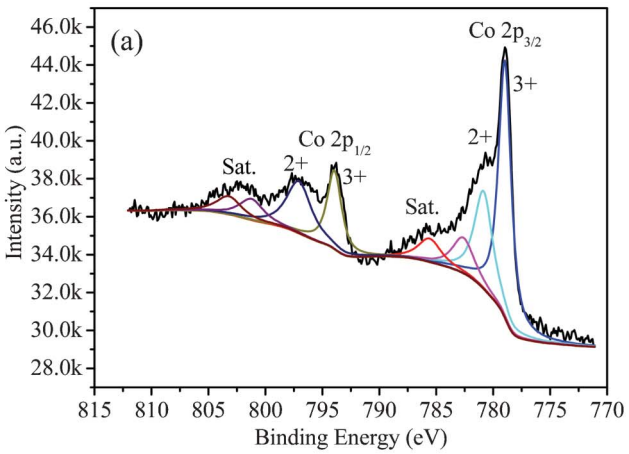


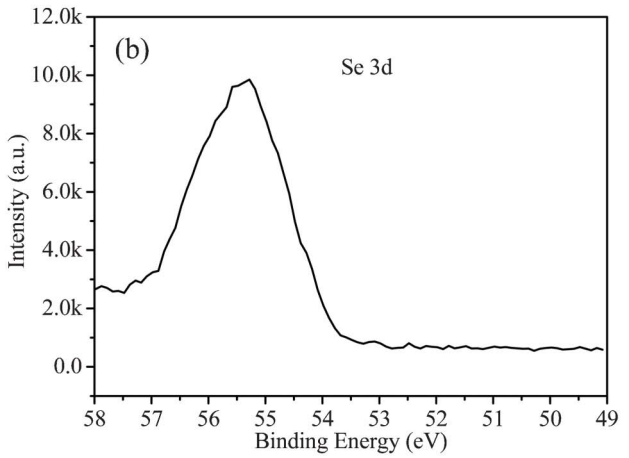


**Fig. 2** XPS core level spectra of (a) the Co 2p region, and (b) the Se 3d region.

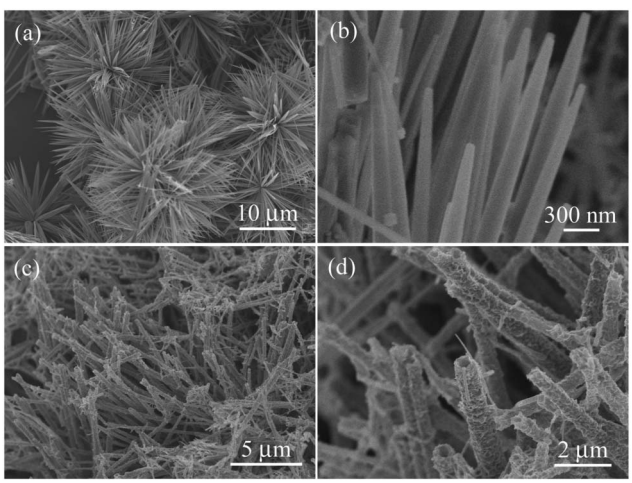


**Fig. 3** (a, b) FESEM images of the precursor $Co(CO_3)_{0.35}Cl_{0.20}(OH)_{1.10}$ sample, and (c, d) the $Co_{0.85}Se$ sample obtained by reacting the precursor with NaHSe solution.

nanorods are needle-like, with diameters of 150–300 nm, and lengths of several micrometers. Fig. 3c shows a FESEM image of the $Co_{0.85}Se$ sample prepared by treating the precursor in NaHSe solution at 140 °C for 8 h. From this image we learn that the as-prepared sample is composed of many rod-like nanomaterials that resemble the precursor. However, a FESEM image (Fig. 3d) with higher magnification shows that the rod-like nanomaterials are actually nanotubes. Some of the nanotubes are broken, and their open ends can be clearly seen. The surfaces of the nanotubes are very rough because the nanotubes are polycrystalline and are composed of many tiny nanoparticles. From the comparison of the morphologies of the precursor and final $Co_{0.85}Se$ sample, it is reasonable to conclude that the precursor serves as a sacrificial template for the preparation of $Co_{0.85}Se$ nanotubes.

The morphology and microstructure of the as-prepared $Co_{0.85}Se$ sample was further examined by TEM and HRTEM. Fig. 4a shows a TEM image of the nanotubes, and the hollow structure of $Co_{0.85}Se$ nanotubes can be clearly seen. Fig. 4b gives a SAED pattern of a $Co_{0.85}Se$ nanotube, in which several diffraction rings are seen, suggesting that the $Co_{0.85}Se$ nanotube is polycrystalline. Fig. 4c is a HRTEM image taken at the side of a $Co_{0.85}Se$ nanotube. The observed interplanar spacing is 0.27 nm, which corresponds to the separation between (101) lattice planes of $Co_{0.85}Se$. The elemental composition of the $Co_{0.85}Se$ nanotube is further confirmed by EDX analysis. EDX spectrum of the $Co_{0.85}Se$ nanotube shown in Fig. 4d indicates the presence of Co, Se as well as C, Cu and Cr which come from TEM copper grid. This result is consistent with the XRD and XPS analysis.

The prepared $Co_{0.85}Se$ nanotubes can act as an efficient catalyst for the decomposition of hydrazine hydrate. The concentration of hydrazine hydrate was measured using a spectrophotometric method. As hydrazine hydrate is colorless, *p*-dimethylaminobenzaldehyde was applied as a chromogenic agent in acidic conditions to form a yellow hydrazone with an absorption maximum at 456 nm. Fig. 5a shows the time-dependent UV-vis absorption spectra of a hydrazine hydrate aqueous solution with *p*-dimethylaminobenzaldehyde as chromogenic agent in the presence of $Co_{0.85}Se$ nanotubes as decomposition catalyst. The intensity of the absorption peak centered at 456 nm gradually decreases with increasing time due to the concentration decreasing of hydrazine hydrate. This result indicates that hydrazine hydrate is gradually degraded with the presence of $Co_{0.85}Se$ nanotubes as decomposition catalyst. The decomposition rate of hydrazine hydrate reaches over 90% after 30 min. Fig. 5b shows the comparison of the catalytic efficiency between $Co_{0.85}Se$ nanotubes and nanoparticles. It is obvious that $Co_{0.85}Se$ nanotubes have higher catalytic activity. After completion of the catalytic reaction, the catalysts were collected by centrifugation without washing, and then were used repeatedly. Fig. 5c shows a comparison of the degradation rates of hydrazine hydrate in the presence of $Co_{0.85}Se$ nanotubes at different cycles. From this figure we learn that the catalytic activity of the $Co_{0.85}Se$ nanotubes is stable during the cycle process.

The capacitances of $Co_{0.85}Se$ nanotubes were characterized in a three-electrode electrochemical cell with 1 M KOH solution as the electrolyte by CV and charge–discharge measurements. Fig. 6a shows the CV curves of the $Co_{0.85}Se$

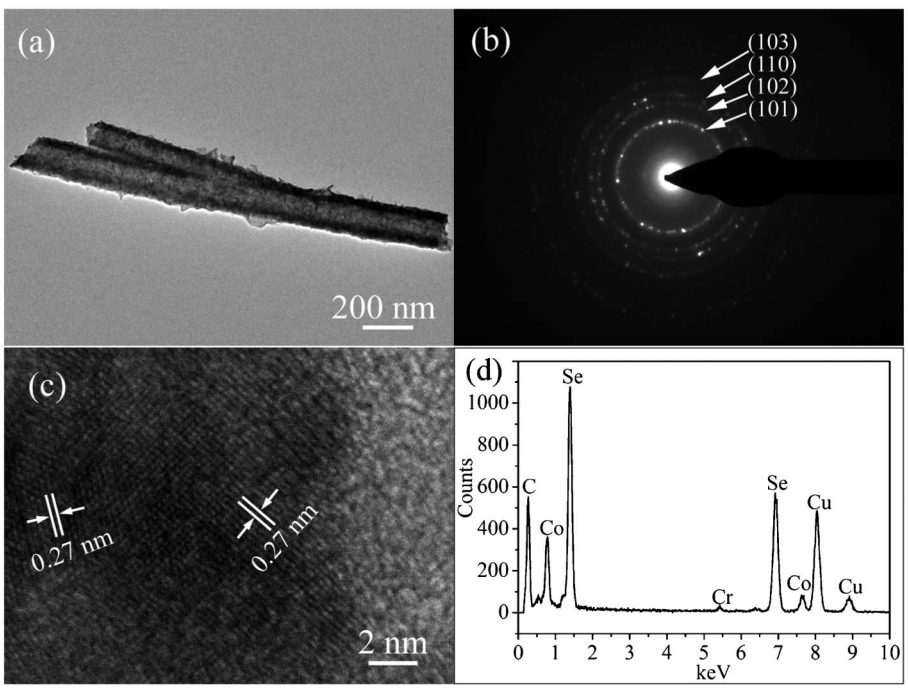


**Fig. 4** (a) TEM image of the $Co_{0.85}Se$ nanotubes; (b) SAED pattern of the $Co_{0.85}Se$ nanotube; (c) HRTEM image of the $Co_{0.85}Se$ nanotube; (d) EDX spectrum of the $Co_{0.85}Se$ nanotube.

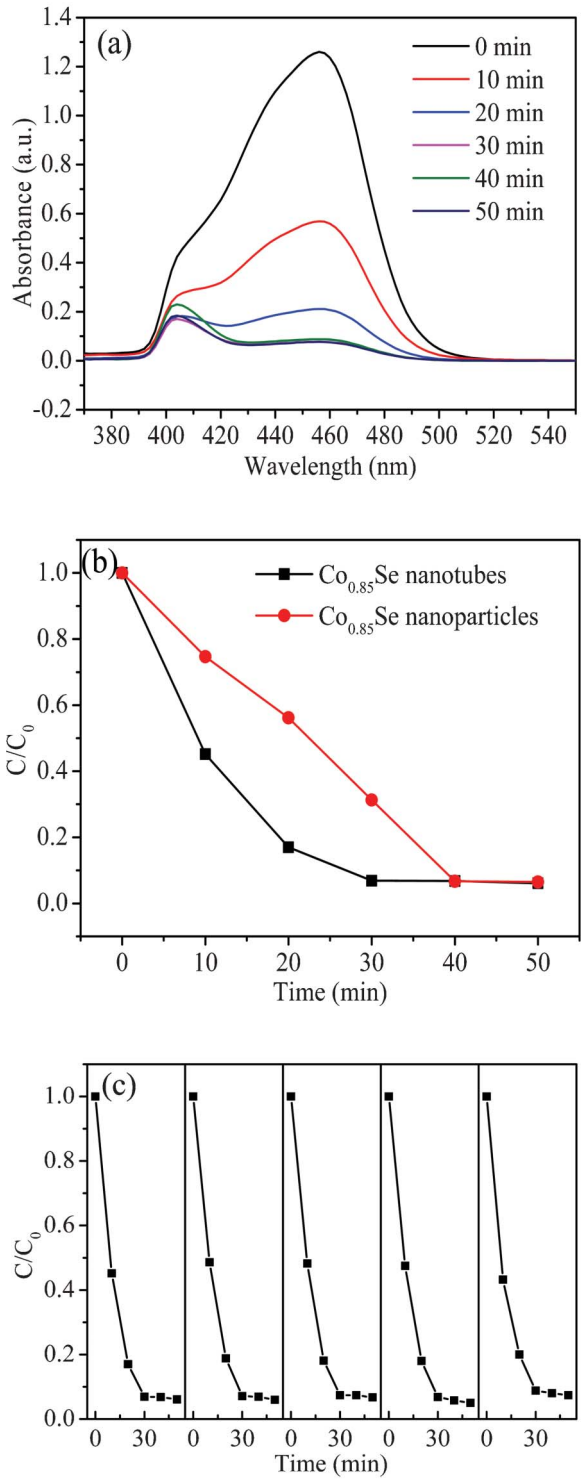


**Fig. 5** (a) Time-dependent absorption spectra of a hydrazine hydrate aqueous solution with *p*-dimethylaminobenzaldehyde as chromogenic agent in the presence of $Co_{0.85}Se$ nanotubes as decomposition catalyst; (b) comparison of the catalytic effect of $Co_{0.85}Se$ nanotubes and nanoparticles; (c) degradation rate of hydrazine hydrate in the presence of $Co_{0.85}Se$ nanotubes at different cycles.

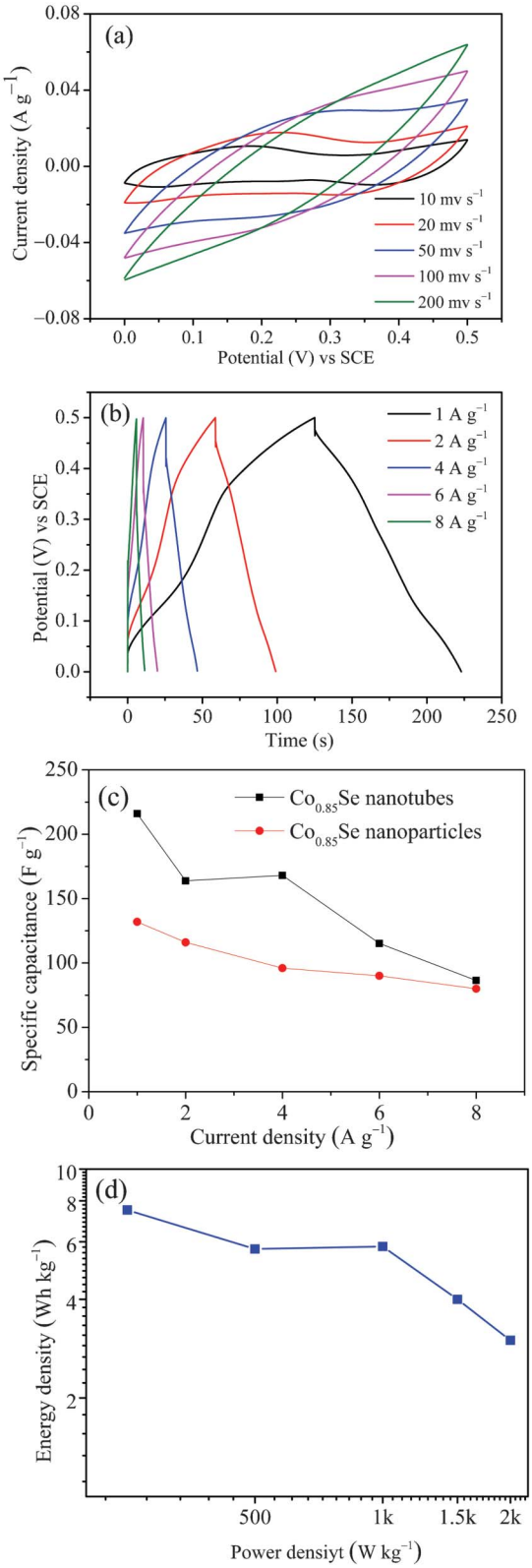


**Fig. 6** (a) CV curves of the $Co_{0.85}Se$ nanotubes electrode at various scan rates; (b) galvanostatic charge–discharging curves of the $Co_{0.85}Se$ nanotubes electrode measured at various current densities; (c) specific capacitances of $Co_{0.85}Se$ nanotubes electrode and $Co_{0.85}Se$ nanoparticle electrode at different discharge current densities; (d) Ragone plots showing energy density *vs.* power density of the $Co_{0.85}Se$ nanotubes electrode.

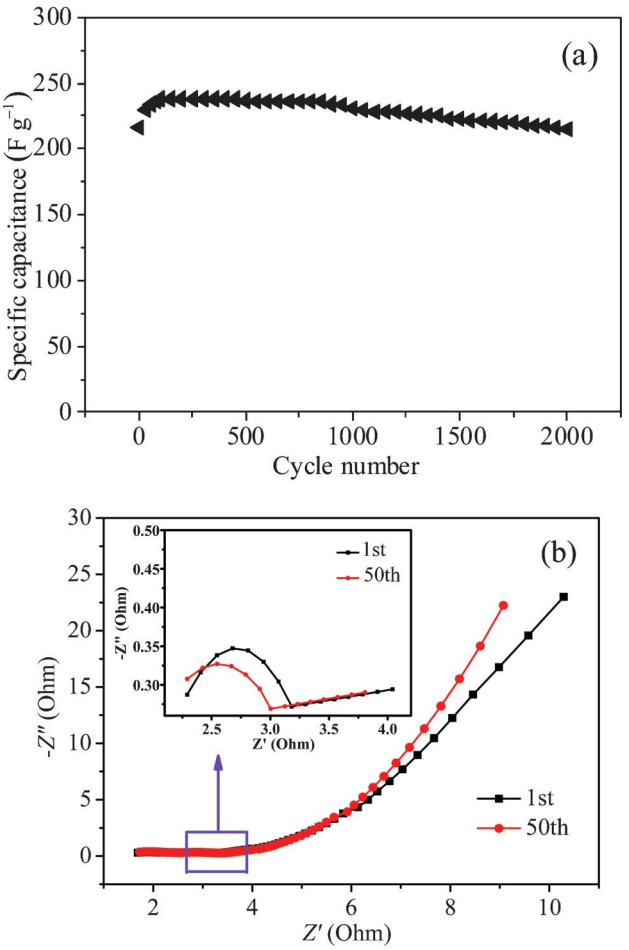


**Fig. 7** (a) Stability test in terms of specific capacitance for the $Co_{0.85}Se$ nanotubes electrode; (b) Nyquist plot of $Co_{0.85}Se$ nanotube supercapacitor cell.

nanotubes electrode at various scan rates from 10 to 200 mV $s^{-1}$. The shapes of the CV curves shown here are different from the CV curves of electric double-layer capacitances that are close to an ideal rectangular shape, indicating that the capacity of $Co_{0.85}Se$ nanotubes results from the pseudocapacitive capacitance.[36,37] The galvanostatic charge–discharge behaviors of the $Co_{0.85}Se$ nanotubes were measured at various current densities (1, 2, 4, 6 and 8 A $g^{-1}$) with a potential window between 0 and 0.5 V, and the corresponding results are shown in Fig. 6b. As expected, the shapes of these charge–discharge curves are nonlinear. The specific capacitances of the $Co_{0.85}Se$ nanotubes calculated from the galvanostatic discharge curves using the formula provided in the Experimental section are 216, 164, 168, 115.2 and 87.4 F $g^{-1}$ at 1, 2, 4, 6 and 8 A $g^{-1}$, respectively, as shown in Fig. 6c. As a comparison, specific capacitances of the $Co_{0.85}Se$ nanoparticles were also measured, which are 132, 116, 96, 90 and 80 F $g^{-1}$ at 1, 2, 4, 6 and 8 A $g^{-1}$, respectively. According to the results, the $Co_{0.85}Se$ nanotubes have a superior capacitive property.

The Ragone plot is commonly utilized to illustrate the energy density (the storage capacity) as a function of power density (the rate of charge/discharge) of electrode materials. The calculations of the energy density and power density are provided in the Experimental section. As shown in Fig. 6d, the $Co_{0.85}Se$ nanotubes has a high energy density of 7.5 Wh $kg^{-1}$ at a power density of 0.25 kW $kg^{-1}$, and a high power density of 2 kW $kg^{-1}$ at an energy density of 3 Wh $kg^{-1}$.

An important requirement for supercapacitor applications is cycling capability or cycling life. To evaluate the stability of the $Co_{0.85}Se$ electrode during the charge–discharge cycles, the values of specific capacitance with respect to charge–discharge cycle number (up to 2000 cycles) at a current density of 1 A $g^{-1}$ are measured, as shown in Fig. 7a. From the curve, the specific capacitance of $Co_{0.85}Se$ electrode was increased from 216 to 238 F $g^{-1}$ after the initial 100 cycles. It is believed that these 100 cycles are needed to fully activate the $Co_{0.85}Se$ material. With increasing cycle number, the specific capacitance slowly decreases and a deterioration of about 9.7% of the maximum specific capacitance occurs after the next 1900 cycles. This result shows that the $Co_{0.85}Se$ electrode has a good long term cyclic performance.

The EIS, also known as Nyquist plot, shows the frequency response of the electrode–electrolyte system and is a plot of the imaginary component of the impedance against the real component. The impedance of the $Co_{0.85}Se$ nanotube electrode after the 1st and 50th cycles was measured, as shown in Fig. 7b. In the high frequency domain, a small semicircle is observed, and in the low frequency section, the plot tends to be a straight line where the imaginary part of the impedance rapidly increases. The semicircle in the high frequency range is attributed to the charge-transfer process at the compound–electrolyte interface, and the straight sloping line is related to the diffusive resistance (Warburg resistance) of the electrolyte entering the interior of the electrode pores and ion diffusion into the host materials.[38,39] After 50th cycling, the sloping line becomes more sloping than before, demonstrating that the electrode behaves more closely as an ideal capacitor.

## 4 Conclusions

In summary, polycrystalline $Co_{0.85}Se$ nanotubes with a well-defined hollow structure are successfully prepared through a solvothermal route by using $Co(CO_3)_{0.35}Cl_{0.20}(OH)_{1.10}$ nanorods as sacrificial hard templates. The $Co_{0.85}Se$ nanotubes exhibit superior catalytic activity than $Co_{0.85}Se$ nanoparticles for the decomposition of hydrazine hydrate in aqueous solution at room temperature, and can be used repeatedly with stable catalytic performance. The $Co_{0.85}Se$ nanotubes can also be applied as electrode materials for electrochemical supercapacitors. Electrochemical measurements validate the excellent pseudocapacitive properties with high specific capacitance, excellent cycle stability and high rate capability that are superior to $Co_{0.85}Se$ nanoparticles. Therefore, the good catalytic and electrochemical properties of the $Co_{0.85}Se$ nanotubes will make them attractive for promising applications in the fields of catalysis and supercapacitors.

## Acknowledgements

Financial supports from the National Natural Science Foundation of China (No. 21171006, 21272006) are gratefully acknowledged.

## Notes and references

1 Y. Q. Lai, F. Y. Liu, J. Yang, B. Wang, J. Li and Y. X. Liu, *Appl. Phys. Express*, 2011, **4**, 071201.
2 Y. J. Feng and N. Alonso-Vante, *Electrochim. Acta*, 2012, **72**, 129.
3 C. C. Liu, J. M. Song, J. F. Zhao, H. J. Li, H. S. Qian, H. L. Niu, C. J. Mao, S. Y. Zhang and Y. H. Shen, *Appl. Catal., B*, 2012, **119–120**, 139.
4 M. R. Gao, S. Liu, J. Jiang, C. H. Cui, W. T. Yao and S. H. Yu, *J. Mater. Chem.*, 2010, **20**, 9355.
5 D. Susac, A. Sode, L. Zhu, P. C. Wong, M. Teo, D. Bizzotto, K. A. R. Mitchell, R. R. Parsons and S. A. Campbell, *J. Phys. Chem. B*, 2006, **110**, 10762.
6 J. F. Zhao, J. M. Song, C. C. Liu, B. H. Liu, H. L. Niu, C. J. Mao, S. Y. Zhang, Y. H. Shen and Z. P. Zhang, *CrystEngComm*, 2011, **13**, 5681.
7 M. Hansen, *Constitution of Binary Alloys*, Geminuim Pub. Co., New York, 1985, p. 502.
8 J. H. Gao, B. Zhang, X. X. Zhang and B. Xu, *Angew. Chem., Int. Ed.*, 2006, **45**, 1220.
9 X. H. Liu, N. Zhang, R. Yi, G. Z. Qiu, A. G. Yan, H. Y. Wu, D. P. Meng and M. T. Tang, *Mater. Sci. Eng., B*, 2007, **140**, 38.
10 J. H. Zhan, X. G. Yang, S. D. Li, Y. Xie, W. C. Yu and Y. Qian, *J. Solid State Chem.*, 2000, **152**, 537.
11 X. Song and M. Bochmann, *J. Chem. Soc., Dalton Trans.*, 1997, 2689.
12 P. Nekooi, M. Akbari and M. K. Amini, *Int. J. Hydrogen Energy*, 2010, **35**, 6392.
13 C. E. M. Campos, J. C. de Lima, T. A. Grandi, K. D. Machado, V. Drago and P. S. Pizani, *Solid State Commun.*, 2004, **131**, 265.
14 F. Y. Liu, B. Wang, Y. Q. Lai, J. Li, Z. A. Zhang and Y. X. Liu, *J. Electrochem. Soc.*, 2010, **157**, D523.
15 Q. Q. Zhou, X. Y. Chen and B. Wang, *Microporous Mesoporous Mater.*, 2012, **158**, 155.
16 X. Y. Chen and Q. Q. Zhou, *Electrochim. Acta*, 2012, **71**, 92.
17 Y. Huang, J. J. Liang and Y. S. Chen, *Small*, 2012, **8**, 1805.
18 C. Zheng, W. Z. Qian, C. J. Cui, Q. Zhang, Y. G. Jin, M. Q. Zhao, P. H. Tan and F. Wei, *Carbon*, 2012, **50**, 5167.
19 Y. Q. Wu, X. Y. Chen, P. T. Ji and Q. Q. Zhou, *Electrochim. Acta*, 2011, **56**, 7517.
20 J. P. Liu, J. Jiang, C. W. Cheng, H. X. Li, J. X. Zhang, H. Gong and H. J. Fan, *Adv. Mater.*, 2011, **23**, 2076.
21 R. Z. Li, X. Ren, F. Zhang, C. Du and J. P. Liu, *Chem. Commun.*, 2012, **48**, 5010.
22 H. R. Ghenaatian, M. F. Mousavi and M. S. Rahmanifar, *Electrochim. Acta*, 2012, **78**, 212.
23 R. B. Rakhi, W. Chen and H. N. Alshareef, *J. Mater. Chem.*, 2012, **22**, 5177.
24 H. S. Kim, N. Branko and B. N. Popov, *J. Power Sources*, 2002, **104**, 52.
25 X. H. Yang, Y. G. Wang, H. M. Xiong and Y. Y. Xia, *Electrochim. Acta*, 2007, **53**, 752.
26 Y. Zhang, Y. Gui, X. Wu, H. Feng, A. Zhang and L. Wang, *Int. J. Hydrogen Energy*, 2009, **34**, 2467.
27 S. Xiong, C. Yuan, X. Zhang, B. Xi and Y. Qian, *Chem.–Eur. J.*, 2009, **15**, 5320.
28 J. Sun, M. Y. Zheng, X. D. Wang, A. Q. Wang, R. H. Cheng, T. Li and T. Zhang, *Catal. Lett.*, 2008, **123**, 150.
29 X. Chen, T. Zhang, M. Zheng, Z. Wu, W. Wu and C. Li, *J. Catal.*, 2004, **224**, 473.
30 Z. H. Wang, X. Y. Chen, M. Zhang and Y. T. Qian, *Solid State Sci.*, 2005, **7**, 13.
31 G. W. Watt and J. D. Chrisp, *Anal. Chem.*, 1952, **24**, 2006.
32 D. Qu and H. Shi, *J. Power Sources*, 1998, **74**, 99.
33 H. Pang, J. W. Deng, J. M. Du, S. J. Li, J. A. Li, Y. H. Ma, J. S. Zhang and J. Chen, *Dalton Trans.*, 2012, **41**, 10175.
34 J. F. Marco, J. R. Gancedo, M. Gracia, J. L. Gautier, E. I. Ríos, H. M. Palmer, C. Greaves and F. J. Berry, *J. Mater. Chem.*, 2001, **11**, 3087.
35 C. D. Wagner, W. W. Riggs, L. E. Davis, J. F. Moulder and G. E. Muilenberg, *Handbook of X-Ray Photoelectron Spectroscopy*, Perkin-Elmer Corporation, Physical Electronics Division, USA, 1979.
36 A. K. Mishra and S. Ramaprabhu, *J. Phys. Chem. C*, 2011, **115**, 14006.
37 R. N. Singh, J. F. Koenig, G. Poillerat and P. Chartier, *J. Electrochem. Soc.*, 1990, **137**, 1408.
38 C. G. Liu, Z. N. Yu, D. Neff, A. Zhamu and B. Z. Jang, *Nano Lett.*, 2010, **10**, 4863.
39 P. Justin and G. R. Rao, *Int. J. Hydrogen Energy*, 2010, **35**, 9709.

 